

Fabrication and characterization of self-organized MnN superstructures on Cu(001) surfaces

Bin Lu,^{*} Xiangdong Liu, Kan Nakatsuji, Takushi Imori, and Fumio Komori[†]

Institute for Solid State Physics, University of Tokyo, Kashiwanoha 5-1-5, Kashiwa-shi, Chiba 277-8581, Japan

(Received 21 May 2007; revised manuscript received 17 August 2007; published 26 December 2007)

A two-dimensional ordered manganese nitride superstructure is prepared by self-organization on the Cu(001). Square MnN islands of a uniform size arrange with a (3.5 ± 0.1) -nanometer periodicity. This structure can be reproducibly fabricated in ultrahigh vacuum chambers by means of atomic nitrogen exposure, Mn deposition, once again atomic nitrogen exposure, and subsequent annealing. Stoichiometry of the island has been determined by *in situ* x-ray photoelectron spectroscopy as a manganese mononitride. In-plane lattice constant of the nanoisland is $\sim 8\%$ larger than that of Cu(001). Deposition of a monolayer manganese upon the MnN superstructure with subsequent annealing up to 690 K gives rise to the same superstructure at the topmost layer. In this case, “MnCu” alloy interlayer is formed between the surface MnN and Cu substrate. The band structures of these films were studied by angle-resolved ultraviolet photoelectron spectroscopy, and the bands due to MnN are identified. The atomic model and formation mechanism of the superstructure are discussed in terms of the strain relief of the lattice in the MnN layers.

DOI: [10.1103/PhysRevB.76.245433](https://doi.org/10.1103/PhysRevB.76.245433)

PACS number(s): 68.65.-k, 68.37.Ef, 68.37.Xy, 73.20.At

I. INTRODUCTION

Periodic nanostructures have been fabricated on crystal surfaces in self-organized ways.¹⁻⁴ These well-ordered nanostructures with uniform size and shape are very suitable both for their detailed characterization in scientific research and low-cost mass production in technological applications. Generally, self-organization at surfaces is driven by strain relief of the lattice nearby the crystal surface. Adsorbates on a crystal surface induce a lattice strain, and long-range repulsive elastic interaction among the nanodomains of the overlayer through the substrate usually plays an important role in the organization.^{5,6} This stress-domain mechanism has well explained most of the observed nanopatterns.⁷ Recently, the authors' group reported a self-organization of manganese nitride nanoisland array on the Cu(001) substrate.⁸ The nanoislands have a square shape and form a two-dimensional square lattice. Interestingly, this nanopattern is not driven by a long-range repulsive elastic interaction but a short-range attractive mechanism.

Manganese nitrides are especially attractive among the 3d transition metal nitrides because of their variety of electronic and magnetic properties, which are suitable for potential applications. These two elements make many kinds of stoichiometric compounds with Mn ions in various valence states.⁹⁻¹³ Moreover, there has been interest in Mn doping of GaN to develop magnetic semiconductor nitride, GaMnN,^{14,15} which could take advantage of unique properties of nitrides, as a source of spin-polarized electrons. Among the manganese nitride compounds, the most N rich one is the mononitride, θ -MnN. Experimentally, the bulk Mn mononitride, which was synthesized by Suzuki *et al.*,¹³ has a tetragonally distorted NaCl structure and is an antiferromagnet with a Néel temperature around 650 K. Recently, a thick MnN film on MgO(001) was grown by Yang *et al.* using molecular beam epitaxy at very low Mn/N flux ratio,¹⁶ whereas theoretical investigations¹⁷⁻²⁰ have proposed several hypothetical crystal structures and magnetic configurations for manganese mononitride. Such structures can be made by heterogeneous epitaxial growths.

In the present paper, we will show detailed experimental results of the MnN on Cu(001) and discuss the growth and

electronic structure of the nanoislands on the Cu(001) substrate. First, we concentrate on the growth behaviors using the results of scanning tunneling microscopy (STM), low-energy electron diffraction (LEED), and *in situ* x-ray photoelectron spectroscopy (XPS). We employed the last to determine its stoichiometry and the interface structure. Next, we discuss the band structures measured by high-resolution angle-resolved ultraviolet photoelectron spectroscopy (ARUPS). The MnN-derived states are identified. Finally, on the basis of these observations, we propose a structural model for the single-layer self-organized islands. The model will easily explain the formation mechanism of the superstructure.

II. EXPERIMENTAL DETAILS

The STM and photoelectron spectroscopy measurements were performed in two independent ultrahigh vacuum (UHV) chambers with the same sample preparation method. The measurement chamber for XPS and ARUPS is equipped with a hemispherical analyzer, a conventional twin anode x-ray source (Al $K\alpha$ and Mg $K\alpha$), a He discharged lamp for ARUPS, and a LEED optics. The x-ray incidence angle was 15° from the surface normal, and the detection angle of the photoelectrons was set at 60° , so that the measurements were surface sensitive. The photon energy for ARUPS is $h\nu = 21.2$ eV (He 1α). Energy and angular resolutions were set to 35 meV and 0.2° , respectively. The sample temperature during the ARUPS measurements and the LEED observation can be changed between 130 and 400 K. Measurements by XPS were performed at room temperature (RT), while ARUPS was obtained at 140 K. Images by STM were recorded in a constant-current mode at RT. It should be pointed out that the orthogonality of all STM images in the present paper has been retrieved after the correction of distortion caused by thermal drift.

The Cu(001) surface was cleaned by several cycles of Ar⁺ ion sputtering and 870 K annealing. The cleanliness of the surface was checked by XPS and Auger electron spectroscopy (AES). Pure manganese (99.98%) was evaporated from

a commercial electron-beam evaporator and the coverage was calibrated by LEED according to the definition that the $\text{Cu}(001)c(2 \times 2)\text{-Mn}$ surface alloy starts from ~ 0.3 ML (monolayer) Mn deposition onto $\text{Cu}(001)$.²¹ Here, 1 ML is defined as one adsorbed atom per substrate atom, corresponding to 1.5×10^{15} atoms cm^{-2} .

The self-organized manganese nitride nanoislands were reproducibly prepared in the following steps. First, the clean substrate surface was exposed to low-energy (150 eV) N^+ bombardment with chamber pressure $= 3 \times 10^{-5}$ Torr at RT for several minutes. Next, 0.9 ± 0.1 ML Mn was deposited on N-adsorbed $\text{Cu}(001)$ substrate at RT. Again, the deposited Mn film was exposed to N^+ with the same condition until saturated, i.e., more than twice of the amount for the nitrogen-saturated $\text{Cu}(001)c(2 \times 2)\text{-N}$ surface. During the exposure to N^+ , the sputtering effect was negligible, as checked by XPS and AES. Finally, the well-ordered nanoislands were spontaneously formed after consecutive annealing the sample in UHV with increasing the temperature from 550 to 670 K gradually for 2 h. It is noted that the deposition sequence of Mn and N has no effect on the final structure and quality of the superstructure. The preparation can alternatively start from depositing Mn on the clean $\text{Cu}(001)$ substrate with subsequent exposure to N^+ . After the sample was annealed with the above mentioned procedure, exactly the same MnN superstructure was achieved. The prepared superstructure is thermally stable at least upon being heated at 820 K for 6 h.

III. RESULTS

A. Superstructure and single-layer growth

Single-layer self-organized nanoislands on $\text{Cu}(001)$ were prepared, as shown in Fig. 1(a) containing 0.9 ± 0.1 ML Mn. The square islands form into a two-dimensional square superstructure with the island side parallel to the square lattice of the substrate Cu crystal. The periodicity of the superstructure is 3.5 ± 0.1 nm, which corresponds to 14×14 $\text{Cu}(001)$ square unit cells. We call this film a single-layer manganese nitride.

An enlarged STM image of the islands is shown in Fig. 1(b). Ignoring the slight distortion, atomic-size protrusions are imaged in a square lattice with the same orientation as the $\text{Cu}(001)$ substrate atoms. In addition, two rows of protrusions are weakly resolved in most of the trenches. By closely looking at the image, each island contains approximately 11×11 protrusions. These indicate a 13×13 periodicity of a square lattice of surface atoms. The 13×13 periodicity of the surface layer and the 14×14 in the Cu substrate are confirmed by the LEED observations.⁸

Stoichiometry of the manganese nitride islands was *in situ* studied by XPS. We employ the well-known nitrogen-saturated $\text{Cu}(001)c(2 \times 2)\text{-N}$ surface as a reference sample for the calibration of the density of N atoms on the surface.²² This surface contains exactly 0.5 ML of N atoms. The spectra from the N-saturated Cu surface and from the surface covered by manganese nitride with 0.9 ML Mn are shown in Fig. 1(c). The integrated N 1s XPS intensity from the single-

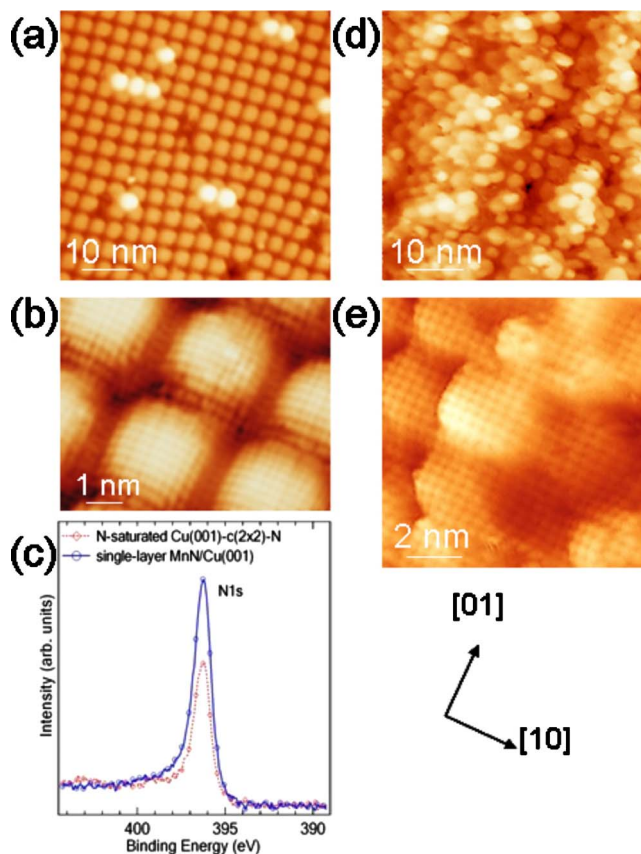


FIG. 1. (Color online) Surface morphologies and stoichiometry of a single-layer manganese nitride on $\text{Cu}(001)$: (a) Large-scale STM image of the single-layer self-organized manganese nitride islands, forming a two-dimensional island superstructure. (b) High-resolution STM image of the self-organized nanoislands showing the atomic-size protrusions. The sample bias voltage is -2 mV and the tunneling current is 0.14 nA. (c) N 1s core level of a N-saturated $\text{Cu}(001)c(2 \times 2)\text{-N}$ surface and the single-layer manganese nitride covered surface. (d) STM topographic image of a disordered MnN single-layer formed by N^+ exposure and 0.9 ML Mn deposition with subsequent light annealing to 563 K for 30 min. (e) Enlarged STM image of (d) shows the local lattice structure.

layer manganese nitride covered surface was reproducibly measured to be 1.8 ± 0.1 times as large as that from the N-saturated surface, i.e., 0.9 ± 0.05 ML N atoms. Thus, 1:1 composition of Mn atoms and N atoms in the manganese nitride is concluded, and the stoichiometry of the manganese nitride is MnN.

As mentioned in the Introduction, a bulk MnN crystal has a face-centered tetragonal structure (a distorted NaCl structure) with the lattice constants of $a = 4.256$ Å and $c = 4.189$ Å.¹³ In the present study, the MnN islands have a structure with in-plane lattice constant $a = 3.89$ Å, which is smaller than the above bulk values. This is not surprising because usually the equilibrium in-plane lattice constant decreases when the film thickness is reduced to monolayer range. For example, an 8% reduction in the lattice constant was found for a single-layer freestanding MgO slab.²³ Consequently, we propose that the present MnN islands adopt a NaCl-like structure as its bulk crystal. The islands consist of

a layer of N atoms with sublattice $\sim 8\%$ larger than that of Cu(001). Manganese atoms are located at the fourfold hollow site of the N sublattice. Lambrecht *et al.*¹⁹ claimed in their theoretical work that electronic states from Mn dominate over the N-derived states near the Fermi level in the MnN bulk crystal. Experimentally, the atomically resolved STM images were obtained only with a small bias. These suggest that the protrusions in the image can be assigned to the Mn atoms. This structural model is consistent with the (1×1) LEED pattern and explains the observed STM results.

As mentioned in Sec. II, the deposition sequence of Mn little affects the final structure. Thus, the annealing process should play an essential role in making the MnN superstructure. To understand the growth and structure of this system better, we studied the morphology after a light annealing. After the N^+ exposure and the 0.9 ML Mn deposition followed by the annealing to 563 K for 30 min, a rough MnN surface appeared, as shown in Fig. 1(d). We can see disordered assemblies of the MnN islands at this stage in the STM image, although this annealing temperature was insufficient for the formation of the ordered superstructure. Moreover, the (1×1) lattice can be identified in an enlarged image in Fig. 1(e), indicating that the disordered surface was fully covered by the single-layer MnN. This agrees with the observation that Cu (1×1) spots and contracted MnN (1×1) spots coexist in the LEED pattern on this surface. The MnN-covered structure after the light annealing can be regarded as the precursor state of the final well-ordered MnN superstructure. At this stage even before forming the superstructure, all nitrogen atoms bond to Mn atoms and a MnN layer covers the surface. With further increasing the annealing temperature and time, the MnN superstructure starts to form and will eventually evolve into a wide and flat surface with the superstructure [Fig. 1(a)] after the heavy annealing above 630 K.

When the Mn coverage is less than 0.9 ML, the MnN-covered surface exhibits a low density of islands with maintaining the size, orientation, and periodicity in the same manner as the full-covered sample.⁸ In addition, embedded areas of MnN, which are adjacent to the MnN islands, are present throughout the growth process in the submonolayer regime, and the lattice in these areas is (1×1) , as shown in the previous Letter.

B. Segregation of MnN layer

Depositing further 0.9 ± 0.1 ML Mn on a single-layer MnN-covered sample at RT in UHV leads to the same superstructure on the topmost surface layer after annealing to 690 K. This has been confirmed by STM and LEED investigations in the following way. Figure 2 shows the evolution of surface morphologies in this process. After deposition of 0.05 ML Mn on a single-layer MnN surface at RT, small Mn clusters are randomly distributed on the top of the MnN islands, as shown in Fig. 2(a). After further deposition of Mn up to ~ 1 ML, the surface became disordered, and the trenches between the islands could no longer be well distinguished, as shown in Fig. 2(b). No distinct morphology change was observed for the sample for over 10 h at RT.

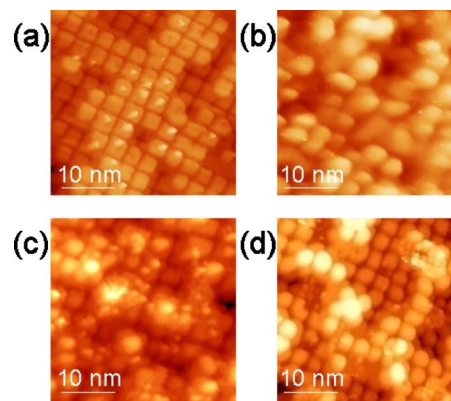


FIG. 2. (Color online) (a) STM image of a surface after deposition of 0.05 ML Mn onto the single-layer MnN superstructure at RT. Small Mn clusters can be seen. [(b)–(d)] Surface morphology evolution after deposition of Mn on the single-layer MnN followed by subsequent annealing. (b) After 1 ML Mn deposition at RT, the surface became disordered. (c) After annealing the sample shown in (b) at 590 K for 1 h, square islands appeared, while most areas of the surface are still covered with disordered clusters. (d) After annealing the sample shown in (c) above 690 K for 1 h, the self-organized MnN island superstructure formed, while few disordered small islands remained.

After an annealing to 590 K for 1 h, the square islands appeared, while the majority of the surface was still covered by disordered clusters [Fig. 2(c)]. An ordered island superstructure is finally achieved after further annealing the sample to 690 K for 1 h, as presented in Fig. 2(d). The LEED investigations also confirmed this evolution. We even obtained the superstructure on the topmost layer by deposition of 4 ML Mn on the prepared single-layer MnN and annealing to 690 K for more than 1 h. The nitrogen atoms of the MnN layer tend to segregate to the surface layer during annealing, as in the case of N-mediated Co film growth on Cu(001).²⁴

Figures 3(a) and 3(b) show the XP spectra of N $1s$ and Cu $2p_{3/2}$. For the MnN film prepared by the above process, a total of ~ 2 ML Mn was deposited on the surface. For convenience, we call this film a single-layer MnN/MnCu/Cu hereafter. We note that the notation “MnCu” here means a mixture of Mn and Cu at the interface, not a stoichiometric alloy. The spectra were recorded with Al $K\alpha$ x-ray source and were normalized by the anode current of the x-ray source in each figure. While the N $1s$ peak was located at 396.3 eV in binding energy on the single-layer MnN/Cu, it showed a core-level shift to 396.6 eV after further 1 ML Mn deposition and the annealing. It is noteworthy that the integrated peak intensity of N $1s$ reduced less than 3% for the latter. Meanwhile, the peak intensity of the Cu $2p_{3/2}$ peak (932.5 eV) decreased to half, as shown in Fig. 3(b). This result confirms that all the N atoms segregated to the surface and formed the MnN superstructure. No other manganese nitride phases were detected in the final stage, while broad peaks were often recorded for insufficiently annealed samples. Manganese nitride species other than MnN are unstable during the complete annealing process. The residual Mn atoms at the subsurface can form “MnCu” alloy with Cu substrate at the interface as that for Mn on clean Cu(001)

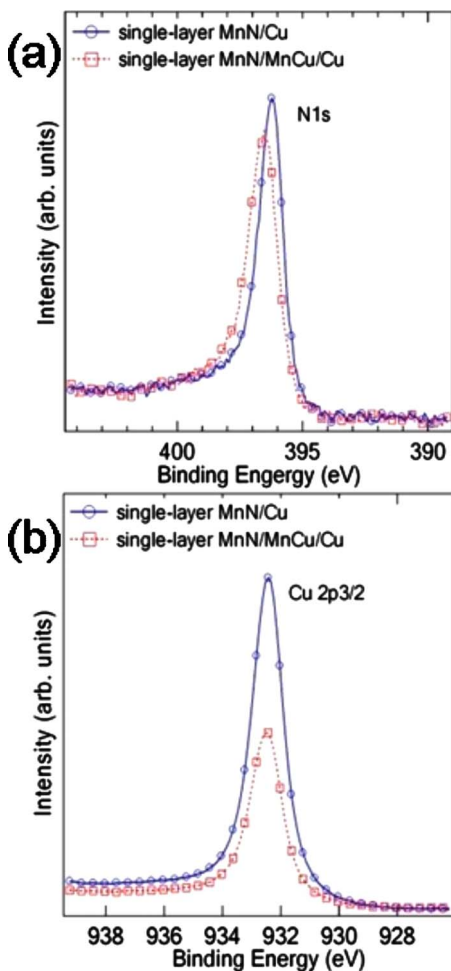


FIG. 3. (Color online) XP spectra of N $1s$ and Cu $2p_{3/2}$ core levels taken on the single-layer MnN/Cu and the single-layer MnN/MnCu/Cu surfaces. (a) N $1s$ core level of these two different MnN-covered surfaces (see annotations inside). Peak shift among them were detected, while no peak shift was observed for their corresponding Cu $2p_{3/2}$ core level (b). The spectra were taken using a photon energy of 1486.6 eV (Al $K\alpha$).

surface. The Cu XPS signal indicates that the Cu concentration in the subsurface layers is significantly low. The presence of the alloy layers (instead of a pure Mn monolayer film) can be verified by Mn XPS and ARUPS measurements, which we will discuss in the following sections.

A peak of N $1s$ in the single-layer MnN/MnCu/Cu was shifted from that in the single-layer MnN/Cu [see Fig. 3(a)], while no chemical shift was detected between the N-saturated Cu(001) surface and the single-layer MnN surface in Fig. 1(c). The latter suggests that Mn atoms offer N atoms the same chemical environment as Cu atoms after bonding with N atoms and forming manganese nitride islands. The distinct chemical shift of N $1s$ in the single-layer MnN/MnCu/Cu is, thus, attributed to the change of the bonding environment with substrate from Cu(001) to the MnCu alloy layer.

The conclusion that the interlayer is a MnCu alloy rather than a pure Mn can be evidenced by investigating the XP spectra of Mn $2p$ core level for all these surfaces. After the

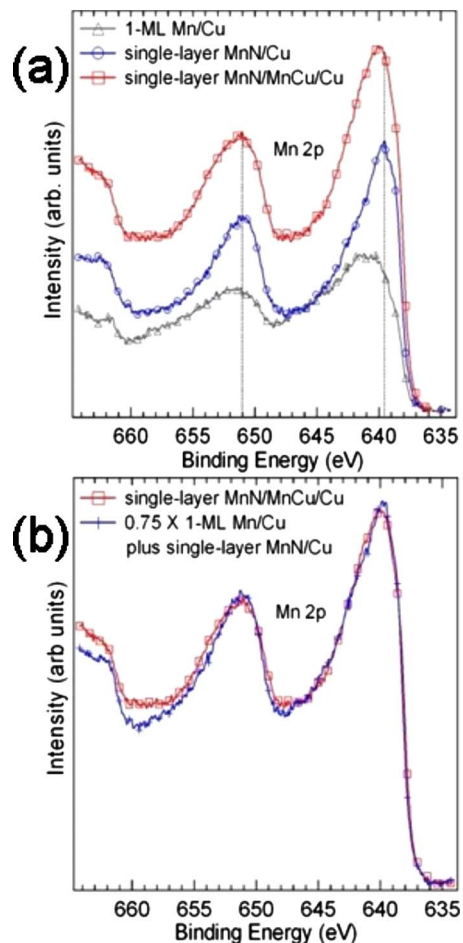


FIG. 4. (Color online) (a) Mn $2p$ core-level spectra for different surfaces (see annotations). (b) A comparison of Mn $2p$ core-level between the single-layer MnN/Cu plus 1 ML Mn/Cu(001) and the single-layer MnN/MnCu/Cu system (for details, see text). The spectra were taken using a photon energy of 1253.6 eV (Mg $K\alpha$).

formation of the MnN overlayer, the peak positions and the line shape of Mn $2p$ change dramatically compared with those from the N-free 1 ML Mn/Cu(001) surface, which was made by Mn deposition at RT containing nominal 1 ML Mn, as shown in Fig. 4(a). For the single-layer MnN/MnCu/Cu, apart from the increase of intensity, the broadening of $2p_{1/2}$ and $2p_{3/2}$ peaks at the higher binding energy region is observed. Based on our XPS measurements of thick (up to 1.8 ML) Mn on Cu(001) (not shown) and a previous report,²⁵ the peak positions of Mn shift to low binding energies and get narrower when increasing the Mn coverage on Cu(001) surface from ~ 1 ML. Thus, we consider that a pure Mn film has a sharp peak at a low binding energy. In our XPS results for the single-layer MnN/MnCu/Cu(001), the broadening of Mn peaks at the higher binding energy region, compared to the single-layer MnN/Cu(001), is an opposite trend and is not an indication of the existence of metallic Mn (a pure Mn monolayer) at the interface, but most likely the formation of the MnCu alloy interlayer. The substantial reduction of the Cu XPS signal for the single-layer MnN/MnCu/Cu(001) is possibly due to the nonuniformity of the Mn_xCu_y layers and

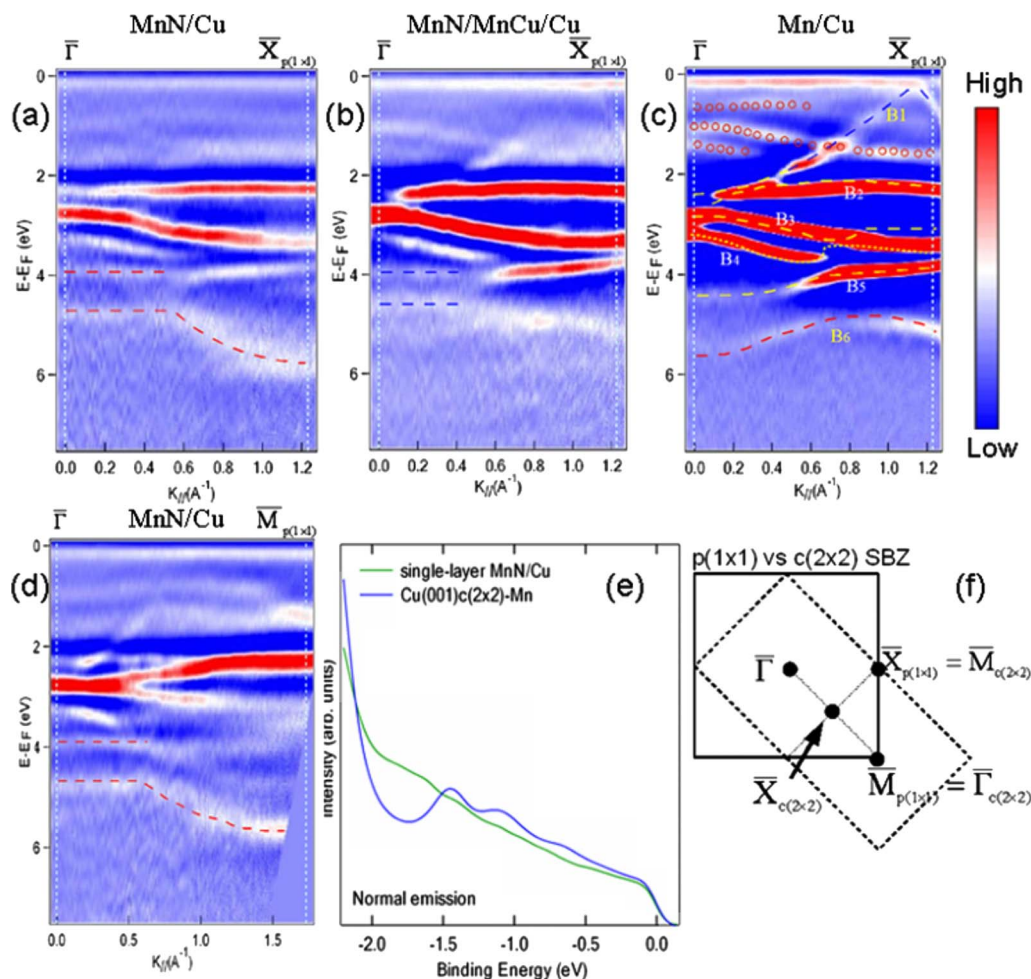


FIG. 5. (Color online) Measured band dispersion in the high-symmetry $\bar{\Gamma}\text{-}\bar{X}_{p(1\times 1)}$ direction for (a) single-layer MnN/Cu(001), (b) single-layer MnN/MnCu/Cu(001), and (c) 1 ML Mn/Cu(001) as well as in the high-symmetry $\bar{\Gamma}\text{-}\bar{M}_{p(1\times 1)}$ direction for (d) single-layer MnN/Cu(001) in a second differential of density plot ($h\nu=21.218$ eV) using the indicated color (gray) scale. The MnN-derived bands in [(a), (b), and (d)] are labeled by red (gray) dashed curves and blue (gray) dashed lines. In (c), the experimental bulk electronic bands of the clean Cu(001) surface as well as ghost signals [induced by He I β (23.09 eV) line] are roughly marked as white dashed curves and open circles, respectively. The positions of $\bar{\Gamma}$, \bar{X} , and \bar{M} are marked in white dotted lines in the corresponding figure. (e) Valence-band spectra recorded at normal emission for the optimum Cu(001)c(2 \times 2)-Mn and for the single-layer MnN/Cu(001) using the same photon energy. (f) Comparison of the p(1 \times 1) to c(2 \times 2) surface Brillouin zone.

the Cu concentration in the upper layer(s) is likely lower.

Moreover, the spectrum of the single-layer MnN/MnCu/Cu(001) can be well reproduced by the superposition of background subtracted Mn 2*p* signals from the 1 ML Mn/Cu(001) and that from the single-layer MnN on the Cu(001) surface, as shown in Fig. 4(b). Here, the intensity ratio is roughly 3:4. This is consistent with the distribution of Mn atoms by considering the attenuated intensity of the signal from the interlayer and is a further indication of alloy layer formation instead of a pure Mn film for the interlayer material. The contribution in the Mn signal from the MnN layer can thus be considered the same in both the single-layer MnN/Cu and the single-layer MnN/MnCu/Cu. In contrast to N atoms, the binding energy of Mn atoms of the MnN layer is independent of the substrate. This conclusion also implies that the interface interaction between the MnN overlayer and the Cu substrate is mainly via N-Cu bonding

rather than Mn-Cu bonding for the single-layer MnN/Cu and is consistent with the subsurface-dependent core-level shift in N 1*s*. For the single-layer MnN/MnCu/Cu, there are both N-Cu and N-Mn(Mn_{*x*}Cu_{*y*}) bondings, and the latter causes the chemical shift shown in Fig. 3(a).

C. Angle-resolved ultraviolet photoelectron spectroscopy measurements

Figures 5(a)–5(c) present the experimentally observed dispersions in a density plot as derived from the second differential of photoemission energy distribution curves at a photon energy of 21.2 eV along $\bar{\Gamma}\text{-}\bar{X}_{p(1\times 1)}$ for the single-layer MnN/Cu system, the single-layer MnN/MnCu/Cu, and 1 ML Mn/Cu, respectively. A color scale is used to indicate the photoemission intensity. The surface Brillouin zones of the

Cu(001)- $p(1 \times 1)$ and the Cu(001) $c(2 \times 2)$ -Mn system are shown in Fig. 5(f).

We compare the MnN ARUPS with those for the extensively-studied Mn/Cu(001) system^{26–29} as we did using the XPS results in the previous section. Well identified bulk electronic bands of the clean Cu(001) surface³⁰ are roughly marked as dashed curves in Fig. 5(c). For the 1 ML Mn/Cu(001) surface, strong emission from Mn 3*d* and the substrate Cu 3*d* bands are observed between 2 and 4.5 eV of binding energy (BE). It is difficult to divide the spectrum into two components from Mn and Cu because of their superposition, as indicated in the previous research of this system.²⁸ The spectra measured in this energy range after Mn deposition have a similar shape to that from the clean surface while the peak positions are shifted slightly. Hence, little attention will be paid to discuss the band changes in this energy range.

Compared to the band structures of the pure Cu(001) and the 1 ML Mn/Cu(001) shown in Fig. 5(c), the MnN overlayer derived states can thus be clearly identified and are labeled by red and blue dashed lines in Figs. 5(a), 5(b), and 5(d). The bands located at around 3.95 and 4.6 eV of BE disperse little at small wave vectors around the $\bar{\Gamma}$ point and are seen for both the single-layer MnN/MnCu/Cu and the single-layer MnN/Cu. Distinctly dispersing bands were observed below 4 eV of BE and $k_{\parallel} > 0.5 \text{ \AA}^{-1}$ for the single-layer MnN/Cu in the both high-symmetry directions, as shown in Figs. 5(a) and 5(d). These originate from the MnN overlayer. However, they were not observed for the single-layer MnN/MnCu/Cu system. This discrepancy is believed to be due to the different interaction between the MnN overlayer and the subsurface for these two cases, as in the previous (XPS) section.

We note that dim structures (labeled open circles) in Fig. 5(c) are attributed to the signals induced by He I β (23.09 eV) from the strong 3*d* states. In the energy range above the Cu 3*d* states, no intrinsic electronic states were clearly detected for the single-layer MnN/Cu(001) and the single-layer MnN/MnCu/Cu(001), as shown in Figs. 5(a), 5(b), and 5(d).

The observed valence electronic structure of the single-layer MnN is different from the calculated result for the bulk MnN crystal.³¹ In the bulk, highly dispersing bands exist between E_F and 2 eV of BE, and even some bands cross the Fermi level. Although the calculated bands between 4 and 6 eV are not fully shown, dispersing rather than flat bands can be seen throughout this region, which is inconsistent with our experimental results.

The metallic state of the MnN overlayer is indicated by the results at E_F . For the single-layer MnN/Cu, its Fermi edge is clearly detected for the normal emission spectrum, as shown in Fig. 5(e), with that for the optimum Cu(001) $c(2 \times 2)$ -Mn surface with 0.5 ML Mn, although the metallic band itself was not detected. In the previous report on this surface,²⁸ the intensity of the Fermi edge at RT is distinctly higher than that for the clean Cu(001) surface at normal emission. Thus, the observed Fermi edge of the single-layer MnN/Cu with the same intensity is the evidence of the metallic state of MnN, which is consistent with the previous

report on a MnN thin film with a resistivity of 135 $\mu\Omega$ cm at RT.³¹

For the 1 ML Mn/Cu(001) surface prepared at RT with nearly 1 ML Mn, van der Kraan and van Kempen claimed that there would be two layers of Cu(001) $c(2 \times 2)$ -Mn in their STM investigation,²⁷ whereas Pan *et al.* proposed another structure: a single Cu(001) $c(2 \times 2)$ -Mn layer followed by disordered MnCu above.²¹ The detailed geometrical structure of this system has little effect on our claims and conclusions. Our LEED patterns show $c(2 \times 2)$ spots (not shown) after the deposition of 1 ML Mn on Cu(001) at RT and thus it is plausible to assume it to be a single Cu(001) $c(2 \times 2)$ -Mn layer with additional MnCu layers above with non-uniform Cu(Mn) concentration in our case.

In the band structures of the single-layer MnN/MnCu/Cu, the feature related to the “dog bone” shaped structure, i.e., with the appearance of B1 as defined in Fig. 5(c), could be partially identified. In addition, the signals appearing around B6 in Fig. 5(b) are similar to those in Fig. 5(c) in the region near the \bar{X} point. However, these were not observed in the spectra from the single-layer MnN/Cu. Consequently, the similarities in bands between the single-layer MnN/MnCu/Cu and the 1 ML Mn/Cu(001) allow us to claim the presence of MnCu alloy layers at the interface for the former, as we have discussed in the previous section. For simplicity, the MnCu layers at the interface are supposed to be a single Cu(001) $c(2 \times 2)$ layer with several Mn_xCu_y layers above and possibly, the upper layer (of the Mn_xCu_y), with the lower Cu concentration, as we have proposed in the XPS section. It is worth pointing out that any other metastable phases (if exist) other than the $c(2 \times 2)$ phase could not survive after annealing above 500 K and cooling down²⁶ and can thus be excluded in our case (annealing up to 700 K).

IV. DISCUSSION

On the basis of the above data and analysis, we will be able to propose a model to interpret the formation mechanism of the MnN island superstructure. It is obvious that the self-organization of the MnN islands cannot be explained by the conventional stress-domain mechanism, in which long-range repulsive elastic interaction rather than attractive interaction between islands via the substrate is crucial for the self-organized growth.⁷ A typical example of stress domains is Pb on Cu(111),³² where, for example, the changing periodicity with Pb coverage is clearly observed. This is in contrast with the observations in the present MnN study. As we described in Sec. III A, the change of the island coverage ranging from submonolayer to monolayer by varying the Mn coverage makes no difference in the periodicity of the MnN island superstructure. There should be another mechanism to stabilize the superstructure, as we have proposed in the last Letter.⁸

Our structural model for the MnN superstructure [for the single-layer MnN/Cu(001) surface] is shown in Fig. 6. In this model, the whole surface, both of the island and of the grid trench, is covered by a single-layer MnN. Within a superstructure period, i.e., a 14×14 Cu unit cell, a square ter-

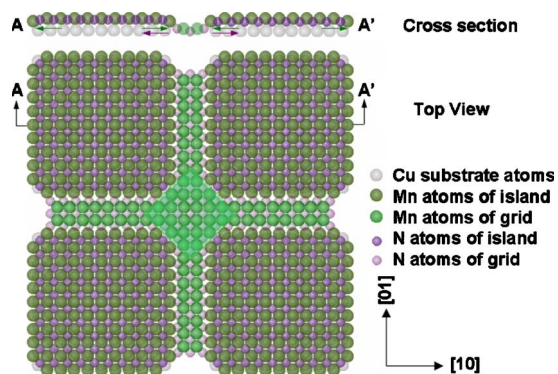


FIG. 6. (Color online) Atomic model of the two-layer-involved self-organization of MnN superstructure based on the STM, LEED, and XPS results. The whole MnN-covered surface splits into two layers. The upper island layer has a lattice constant larger than that of the Cu(001) substrate, while the embedded MnN layer is compressed with the same in-plane lattice constant as the substrate. Mn atoms at the island edges are assumed to buckle downward and bond with the uplifted (buckled upward) N atoms at the trench. The MnN island exerts tensile stress to the topmost Cu layer (labeled green arrows), and the embedded grid imposes compressive stress to that (labeled pink red arrows). Consequently, the stresses balance on the topmost Cu layer underneath the MnN islands. The observed square patch is marked in green transparent unit.

race of the island which contains 10×10 N atoms and 11×11 Mn atoms is located symmetrically onto an 11×11 Cu lattice unit. The remaining monolayer low areas within this cell are also covered by the MnN monolayer and surround the 11×11 Cu lattice in the same layer. This embedded MnN monolayer appears as the grid and is assumed to have the same in-plane lattice constant as the Cu substrate. Thus, these two MnN layers differ in lattice constant. We call this as a two-layer-involved growth model.

As we discussed in the preceding section, the Mn atoms are located at the fourfold hollow site of the N sublattice at the same layer and are imaged as a simple (1×1) lattice. We put Mn atoms at the island edge to make the model consistent with the STM observations. Similarly, we do not place Mn atoms at four corner sites of the island in our model to match it with the STM images. The cross regions (patches) of the grid are always of a square (or a rectangular) shape with its side parallel to the $\langle 11 \rangle$ direction.

The model with this superstructure period, i.e., a 14×14 Cu unit cell, consists of 196 Cu atoms, 175 N atoms, and 173 Mn atoms in the cell. Consequently, the single-layer MnN/Cu surface contains 0.893 ML N, which agrees well with the XPS results shown in Fig. 1(c), i.e., 0.9 ± 0.05 ML N. The amount of Mn deduced from the model is 0.883 ML and is consistent with the definition of the Mn coverage (0.9 ± 0.1 ML) to fabricate a fully MnN-covered surface as well.

The single-layer MnN-covered disordered surface evolved to the final stable island superstructure instead of forming a monolayer compact flat film by annealing. The MnN superstructure is stable even at 820 K. These mean that, compared to the formation of a flat and fully strained MnN overlayer, the two-layer-involved growth is energeti-

cally favored and that the superstructure is thermodynamically equilibrium. Free energy of the whole system should be minimized in the annealing process.

The possible mechanism for the reduction of free energy is as follows. The in-plane lattice of the MnN island is $\sim 8\%$ larger than the Cu substrate. Consequently, the MnN island overlayer tends to expand the underlying Cu(001) lattice, while the MnN grid within this Cu outermost layer has the opposite effect, illustrated as arrows in Fig. 6 (cross section). These two can almost balance with each other and make the Cu substrate lattice nearly unstrained. The increased free energy of the strained MnN grid area can be partially relieved by N atoms buckling upward, as we assumed in the model. The two-layer-involved growth can thus minimize the free energy due to strain.

By this consideration, the size of the MnN islands and the width of the MnN grid are intrinsically defined by the strain equilibrium and are hence independent of the MnN island coverage. It is worth pointing out that, during the self-organization of the superstructure, the MnN patch formation should be either prior to or at the same time as the formation of the MnN islands. Embedded MnN square patches adjacent to the MnN islands are actually seen in the STM images of the surface partially covered by the MnN islands.⁸ The simultaneous appearance of the MnN islands with the adjacent embedded MnN patches is essential for the self-organization of nanoisland superstructure, as we proposed in the previous Letter.

During the annealing after deposition of Mn on the single-layer MnN/Cu, a well-ordered MnN superstructure first decayed, then the nitrogen atoms segregated to surface layer and bonded with the Mn atoms. At the same time, the residual Mn atoms in the subsurface formed MnCu alloy with the Cu substrate. The two-layer-involved growth model can also be employed for the segregation of the MnN overlayer. The MnN under Mn atoms should be unstable because of the compressive stress by the Mn overlayer. The two-layer-involved growth lowers the total free energy of the system irrespective of the presence of Mn atoms in the subsurface. The difference should arise from the interaction between the MnN layer and the subsurface; there are both N-Cu and N-Mn(Mn_xCu_y) bonding in this case, while it is mainly via N-Cu bonding for the single-layer MnN/Cu, as indicated by the results of XPS.

V. CONCLUSIONS

A high-quality two-dimensional array of ordered manganese nitride islands is fabricated by means of self-organization. The stoichiometry of the prepared sample was determined *in situ* as MnN by XPS. The square MnN islands keep their size, shape, and periodicity even when the Mn coverage is less than 0.9 ML. Deposition of up to 4 ML Mn on a single-layer MnN-covered surface followed by annealing results in the formation of the same superstructure on the topmost layer and of MnCu alloy layers at the interface. The XPS results indicate that N atoms of the MnN overlayer play an essential role when bonding with the substrate and

forming the superstructure. The electronic structures due to MnN overlayer were partly identified by ARUPS measurements and its metallic behavior was clarified. We proposed a structural model for the single-layer self-organized islands and the two-layer-involved growth. The segregated MnN layer with MnCu alloy at the interface can also be illustrated by this model.

ACKNOWLEDGMENTS

The authors are indebted to the fruitful experimental collaboration in the XPS and ARUPS measurement by Dai-ichiro Sekiba. This work is partly supported by a Grant-in-Aid from the Ministry of Education, Culture, Sports, Science and Technology, Japan.

*phylu@issp.u-tokyo.ac.jp

†komori@issp.u-tokyo.ac.jp

- ¹K. Thürmer, R. Q. Hwang, and N. C. Bartelt, *Science* **311**, 1272 (2006).
- ²M. Corso, W. Auwärter, M. Muntwiler, A. Tamai, T. Greber, and J. Osterwalder, *Science* **303**, 217 (2004).
- ³H. Brune, M. Giovannini, K. Bromann, and K. Kern, *Nature (London)* **394**, 451 (1998).
- ⁴A. Varykhalov, C. Biswas, W. Gudat, and O. Rader, *Phys. Rev. B* **74**, 195420 (2006).
- ⁵V. I. Marchenko, *JETP Lett.* **33**, 381 (1981).
- ⁶O. L. Alerhand, D. Vanderbilt, R. D. Meade, and J. D. Joannopoulos, *Phys. Rev. Lett.* **61**, 1973 (1988).
- ⁷V. A. Shchukin and D. Bimberg, *Rev. Mod. Phys.* **71**, 1125 (1999).
- ⁸X. D. Liu, B. Lu, T. Iimori, K. Nakatsuji, and F. Komori, *Phys. Rev. Lett.* **98**, 066103 (2007).
- ⁹F. Lihl, P. Etmayer, and A. Kuzelnigg, *Z. Metallkd.* **53**, 715 (1962).
- ¹⁰M. Mekata, J. Haruna, and H. Takei, *J. Phys. Soc. Jpn.* **25**, 234 (1968).
- ¹¹M. Eddine, *Acta Crystallogr., Sect. B: Struct. Sci.* **33**, 2696 (1991).
- ¹²H. Yang, A. R. Smith, M. Prikhodko, and W. R. L. Lambrecht, *Phys. Rev. Lett.* **89**, 226101 (2002).
- ¹³K. Suzuki, Y. Yamaguchi, T. Kaneko, H. Yoshida, Y. Obi, H. Fujimori, and H. Morita, *J. Phys. Soc. Jpn.* **70**, 1084 (2001).
- ¹⁴T. Dietl, H. Ohno, F. Matsukura, J. Cibert, and D. Ferrand, *Science* **287**, 1019 (2000).
- ¹⁵M. L. Reed, N. A. El-Masry, H. H. Stadelmaier, M. K. Ritums, M. J. Reed, C. A. Parker, J. C. Roberts, and S. M. Bedair, *Appl. Phys. Lett.* **79**, 3473 (2001).
- ¹⁶H. Yang, H. Al-Britthen, E. Trifan, D. C. Ingram, and A. R. Smith, *J. Appl. Phys.* **91**, 1053 (2002).
- ¹⁷M. S. Miao and W. R. L. Lambrecht, *Phys. Rev. B* **71**, 214405 (2005).
- ¹⁸H. Shimizu, M. Shirai, and N. Suzuki, *J. Phys. Soc. Jpn.* **66**, 3147 (1997).
- ¹⁹W. R. L. Lambrecht, M. Prikhodko, and M. S. Miao, *Phys. Rev. B* **68**, 174411 (2003).
- ²⁰A. Janotti, S. H. Wei, and L. Bellaiche, *Appl. Phys. Lett.* **82**, 766 (2003).
- ²¹W. Pan, R. Popescu, H. L. Meyerheim, D. Sander, O. Robach, S. Ferrer, M. T. Lin, and J. Kirschner, *Phys. Rev. B* **71**, 174439 (2005).
- ²²F. M. Leibsle, S. S. Dhesi, S. D. Barrett, and A. W. Robinson, *Surf. Sci.* **317**, 309 (1994).
- ²³L. Giordano, J. Goniakowski, and G. Pacchioni, *Phys. Rev. B* **67**, 045410 (2003).
- ²⁴D. Sekiba, S. Doi, K. Nakatsuji, and F. Komori, *Surf. Sci.* **590**, 138 (2005).
- ²⁵Y. Huttel, F. Schiller, J. Avila, and M. C. Asensio, *Phys. Rev. B* **61**, 4948 (2000).
- ²⁶T. Flores, M. Hansen, and M. Wuttig, *Surf. Sci.* **279**, 251 (1992).
- ²⁷R. G. P. van der Kraan and H. van Kempen, *Surf. Sci.* **338**, 19 (1995).
- ²⁸O. Rader, W. Gudat, C. Carbone, E. Vescovo, S. Blügel, R. Kläsges, W. Eberhardt, M. Wuttig, J. Redinger, and F. J. Himpsel, *Phys. Rev. B* **55**, 5404 (1997).
- ²⁹F. Schiller, S. V. Halilov, and C. Laubschat, *Phys. Rev. B* **67**, 214431 (2003).
- ³⁰C. Baldacchini, L. Chiodo, F. Allegretti, C. Mariani, M. G. Betti, P. Monachesi, and R. Del Sole, *Phys. Rev. B* **68**, 195109 (2003).
- ³¹S. Granville, B. J. Ruck, F. Budde, A. Koo, J. E. Downes, H. J. Trodahl, A. Bittar, N. Strickland, G. V. M. Williams, W. R. L. Lambrecht, T. Learmonth, K. E. Smith, V. J. Kennedy, A. Markwitz, and T. Schmitt, *Phys. Rev. B* **72**, 205127 (2005).
- ³²R. Plass, J. A. Last, N. C. Bartelt, and G. L. Kellogg, *Nature (London)* **412**, 875 (2001).